

Control of electron trapping effects in graphene quantum dots via light polarization state

Adrian Pena

National Institute of Materials Physics, Atomîştilor 405A, 077125 Măgurele – Ilfov, Romania

We theoretically analyze the scattering process of an electron on a graphene quantum dot (GQD) exposed to an external light irradiation. We prove that for suitable choices of the light polarization state, there emerge scattering resonances, characterized by electron trapping effects inside the GQD.

I. INTRODUCTION

The first fabrication of graphene in 2004 [1] was the starting point of a new era of solid state physics research. Until today, a colossal number of studies have been performed and the findings were fabulous. One of the most exciting processes which manifests in graphene is so-called *Klein tunneling* [2]. It is a relativistic behavior of charged particles, which consists in the perfect tunneling through a potential barrier, irrespective of its magnitude [3]. Therefore, due to this phenomenon, a permanent localization of an electron inside a graphene system is not achievable. However, there is a number of publications which related about the possibility to trap electrons in graphene quantum dots (GQDs) for finite periods of time [4–14]. These states we discuss about here are called *quasi-bound states*. Moreover, we have argued in a recent paper [11] that circularly polarized light irradiation excites quasi-bound states in a GQD.

In this work, we prove that adjusting the *polarization state* and intensity of the light, we can also successfully control the excitation of quasi-bound states. Graphene was repeatedly proposed as a good candidate for new (opto)electronic devices, due to its striking properties. Hence, the present work may constitute a building block for a new such device and could pave the way towards the so awaited implementation of graphene in everyday technology.

II. THEORY

In low-excitation regime, the charged particles in graphene behave as free massless Dirac fermions [15], namely massless particles moving freely with Fermi velocity $v_F = c/300$, with c being the speed of light in vacuum. First, let us investigate the interaction of a free massless Dirac fermion with an arbitrarily polarized light beam (see Supplementary information 1 for detailed derivations) [16].

The process in question is described by the time-dependent 2D massless Dirac equation [17] (we use polar coordinates):

$$H(r, \varphi, t)\psi(r, \varphi, t) = i\hbar\partial_t\psi(r, \varphi, t); \quad (1)$$

$$H(r, \varphi, t) = H_0(r, \varphi) + H_{int}(t); \quad (2)$$

$$H_0(r, \varphi) = -iv_F\hbar\boldsymbol{\sigma} \cdot \nabla; \quad (3)$$

$$H_{int}(t) = -ev_F\boldsymbol{\sigma} \cdot \mathbf{A}(t). \quad (4)$$

Here, $H(r, \varphi, t)$ is the full Hamiltonian, where $H_0(r, \varphi)$ represents the free Hamiltonian with \hbar being the reduced Planck constant and, respectively, $\nabla \equiv (\partial_r, \frac{1}{r}\partial_\varphi)$ the gradient operator. The second term $H_{int}(t)$, with e the elementary charge,

introduces the interaction with light. $\boldsymbol{\sigma} = (\sigma_r, \sigma_\varphi)$ denotes the Pauli vector, having the following components [18]:

$$\sigma_r = \begin{pmatrix} 0 & e^{-i\varphi} \\ e^{i\varphi} & 0 \end{pmatrix}; \quad \sigma_\varphi = \begin{pmatrix} 0 & -ie^{-i\varphi} \\ ie^{i\varphi} & 0 \end{pmatrix}. \quad (5)$$

The vector potential of the light in plane wave representation for the case of an arbitrarily polarization reads

$$\mathbf{A}(t) = A_0 \left\{ \left[\cos(\omega t) + \xi \cos(\omega t + \theta) \right] \hat{x} + \left[-\sin(\omega t) + \xi \sin(\omega t + \theta) \right] \hat{y} \right\} \quad (6)$$

Here, A_0 is a real constant amplitude, ω the light frequency, \hat{x} and \hat{y} are respectively the unit vectors along the x - and y -axis. Generally speaking, $\mathbf{A}(t)$ describes an elliptical state of polarization.

The polarization ellipse is characterized as follows: ξ indicates the ratio of the principal axes by $|(1+r)(1-r)|$ and θ is a phase term which determines the orientation of the ellipse. As particular cases, for $\xi = 0$ the polarization becomes circular and, respectively, for $\xi = 1$ linear.

Since the Hamiltonian (2) is periodic in time due to the interaction term (4), we employ the Floquet formalism [19–23]. See Supplementary Information 1 [16] for a detailed discussion. For the case of a non-resonant regime, characterized by a much higher energy of the applied light with respect to the energy scale of the Dirac fermion, the problem reduces to an eigenvalue equation associated to the stationary *effective Floquet Hamiltonian*

$$H_F^{eff}(r, \varphi) = H_0(r, \varphi) + \frac{1}{\hbar\omega} [H_{-1}(r, \varphi), H_1(r, \varphi)]; \quad (7)$$

$$H_n(r, \varphi) = \frac{1}{T} \int_0^T e^{in\omega t} H_{int}(r, \varphi, t) dt; \quad T = \frac{2\pi}{\omega}. \quad (8)$$

The first term within Eq. (7) represents the the Hamiltonian (2) averaged over a period T of the light, while the second term of the effective Floquet Hamiltonian expresses the virtual process of absorption/emission of one photon and the commutator is readily derived as

$$[H_{-1}(r, \varphi), H_1(r, \varphi)] = -(ev_F A_0)^2 (\xi^2 - 1) \sigma_z. \quad (9)$$

Now we deal with the following eigenvalue equation for the unknown state spinor $\phi(r, \varphi)$:

$$[H_F^{eff}(r, \varphi) - W]\phi(r, \varphi) = 0, \quad (10)$$

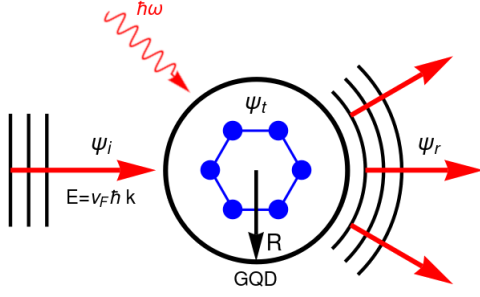


FIG. 1. Sketch of the studied system. The incident electron with energy $E = v_F \hbar k$ is propagating from left towards a GQD of radius R exposed to a light irradiation ($\hbar\omega$). The incident, reflected and transmitted waves are respectively ψ_i , ψ_r , and ψ_t .

where W is the so-called *quasienergy*. Taking into account the results presented above, Eq. (10) translates as

$$\left[-i \left(\sigma_r \partial_r + \frac{1}{r} \sigma_\varphi \partial_\varphi \right) - \frac{1}{\lambda_{A_0}} (\xi^2 - 1) \sigma_z - \kappa \right] \phi(r, \varphi) = 0, \quad (11)$$

where we have introduced the notations $\lambda_{A_0} = \left(\frac{v_F e^2 A_0^2}{\hbar^2 \omega} \right)^{-1}$ and $\kappa = \frac{W}{v_F \hbar}$. Note that the interaction of a free Dirac fermion with light is not affected by θ .

Since the effective Floquet Hamiltonian (7) is rotational invariant, it commutes with the total angular momentum operator $J_z = L_z + S_z$, with $L_z = -i\hbar \partial_\varphi$ being the orbital angular momentum operator and, respectively, $S_z = (1/2)\hbar \sigma_z$ the spin operator. Thus, we have $[H_F^{eff}, J_z] = 0$. Having in mind this relation, we derive the unknown spinor as

$$\phi(r, \varphi) = \begin{pmatrix} \chi_A(r) e^{i l \varphi} \\ i \chi_B(r) e^{i(l+1)\varphi} \end{pmatrix}; \quad (12)$$

$$\chi_A(r) = J_l \left(-i \frac{r \sqrt{\lambda_{A_0}^2 k^2 - (\xi^2 - 1)^2}}{\lambda_{A_0}} \right); \quad (13)$$

$$\chi_B(r) = \frac{\lambda_{A_0} k + \xi^2 - 1}{\sqrt{\lambda_{A_0}^2 k^2 - (\xi^2 - 1)^2}} J_{l+1} \left(-i \frac{r \sqrt{\lambda_{A_0}^2 k^2 - (\xi^2 - 1)^2}}{\lambda_{A_0}} \right). \quad (14)$$

In Eqs. (13) and (14), $J_l(x)$ denotes the first kind Bessel functions of order l .

Let us investigate the following scattering process. We consider an electron propagating towards a GQD of radius R , at normal incidence. The energy of the incident electron is $E = v_F \hbar k$, with k being the associated wave number. After interaction, the electron is either reflected, or transmitted inside the dot. The process is schematically described in Fig. 1. The incident and, respectively, reflected waves involved in the

studied process read with the following equations:

$$\psi_i(r, \varphi) = \frac{1}{\sqrt{2}} e^{i k r \cos \varphi} \begin{pmatrix} 1 \\ 1 \end{pmatrix} = \frac{1}{\sqrt{2}} \sum_{l=-\infty}^{\infty} i^l \begin{pmatrix} J_l(kr) e^{i l \varphi} \\ i J_{l+1}(kr) e^{i(l+1)\varphi} \end{pmatrix}; \quad (15)$$

$$\psi_r(r, \varphi) = \frac{1}{\sqrt{2}} \sum_{l=-\infty}^{\infty} i^l c_l^r \begin{pmatrix} H_l(kr) e^{i l \varphi} \\ i H_{l+1}(kr) e^{i(l+1)\varphi} \end{pmatrix}. \quad (16)$$

Note that Eq. (15) represents a plane wave and was expressed as an infinite sum of well-defined orbital angular momentum states using Jacobi-Anger expansion. Eq. (16) represents the partial waves decomposition of the reflected wave, where $H_l(x)$ denotes the first kind Hankel functions of order l [24]. Based on the Dirac equation solutions derived above [(12)–(14)], the transmitted wave reads

$$\psi_t(r, \varphi) = \sum_{l=-\infty}^{\infty} c_l^t \begin{pmatrix} \chi_A(r) e^{i l \varphi} \\ i \chi_A(r) e^{i(l+1)\varphi} \end{pmatrix}. \quad (17)$$

Now, imposing the continuity condition for the wave functions on the boundary of the GQD

$$\psi_i(R, \varphi) + \psi_r(R, \varphi) = \psi_t(R, \varphi), \quad (18)$$

for $\kappa = k$ by the virtue of energy conservation, the reflection and, respectively, transmission coefficients are readily derived as

$$c_l^t = \frac{\sqrt{2} e^{i \frac{(l+1)\pi}{2}}}{\pi k R [H_l(kR) \chi_B(R) - H_{l+1}(kR) \chi_A(R)]}; \quad (19)$$

$$c_l^r = \frac{J_l(kR) \chi_B(R) - J_{l+1}(kR) \chi_A(R)}{H_{l+1}(kR) \chi_A(R) - H_l(kR) \chi_B(R)}. \quad (20)$$

Going further, for a quantitative description of the scattering, we introduce the scattering efficiency

$$Q = \frac{4}{kR} \sum_{l=-\infty}^{\infty} |c_l^r|^2, \quad (21)$$

defined as the scattering cross section divided by the geometric cross section [25, 26].

III. RESULTS AND DISCUSSION

In what follows we present a numerical analysis of the scattering efficiency for the case of $\omega = 5 \times 10^{14} \text{ s}^{-1}$, $R = 100 \text{ nm}$ and $E = 20 \text{ meV}$. The investigation is performed in terms of ξ and light intensity $I_L = \epsilon_0 \omega^2 A_0^2$, with $\epsilon_0 = 8.854 \times 10^{-12} \text{ Fm}^{-1}$ being the vacuum permittivity.

As depicted in Fig. 2(a) the scattering efficiency presents a very rich pattern, showing interesting magnitude oscillations. As a first observation, we note that the process is very sensitive to the variation of the considered parameters, therefore both polarization and light intensity may be useful tools to control the scattering effect. In what follows, we perform the investigation only with respect to the polarization state, keeping I_L constant. In Fig 2(b) we show Q as a function of ξ for

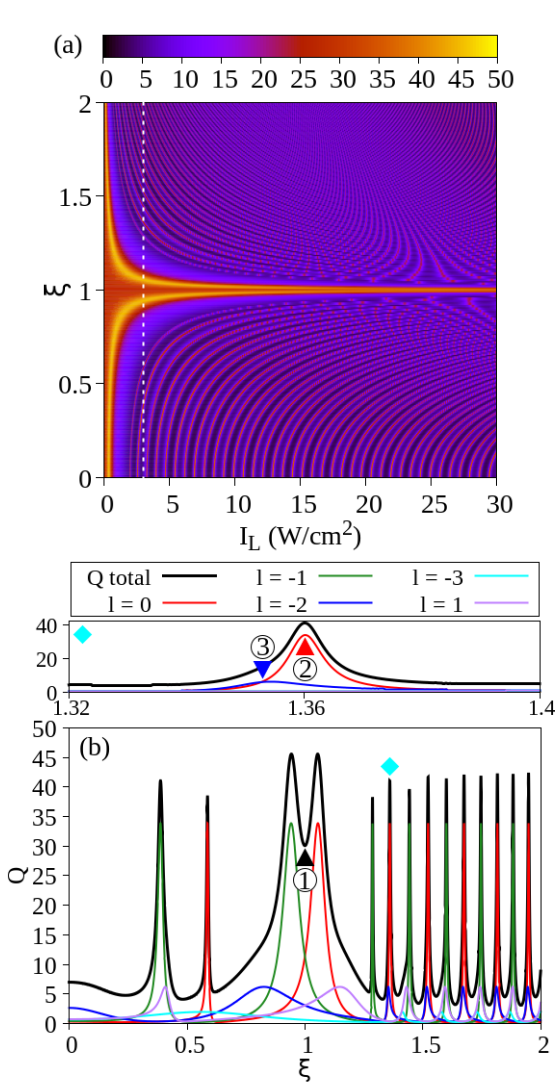


FIG. 2. Scattering efficiency (Q) analysis. (a) Q as a function of light polarization ξ and light intensity I_L . (b) Q as a function of ξ for a constant $I_L = 3$ W/cm^2 [along white dashed line within panel (a)].

$I_L = 3$ W/cm^2 [along dashed white line in Fig. 2(a)]. In the corresponding plot, a series of *scattering resonances* may be observed. Moreover, each scattering resonance is composed by other peaks, each of them associated to a given angular momentum state, called in what follows *scattering mode*. Firstly, we observe that for $\xi = 1$ (linear polarization) the scattering efficiency has a local minimum [see marker 1 (black)]. Hence, in this *non-resonant* regime we do not expect to fetch any trapping effect. Now, we chose to inspect the resonance peak indicated by cyan marker and detailed presented in the upper panel. Contrastingly, in this regime, there are *resonantly* excited two scattering modes, $l = 0$ (red curve) and $l = -2$ (blue curve). Obviously, the $l = 0$ mode is dominant from the point of view of its amplitude. On the other hand, a subsidiary perspective from which the scattering process may be analyzed is in terms of scattering resonance peak shape. In the case of

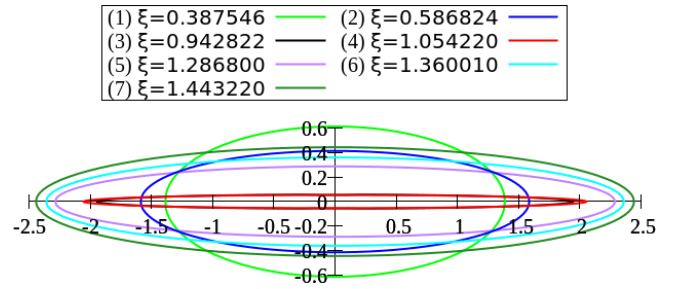


FIG. 3. Polarization ellipses for the first seven resonance peaks presented in Fig. 2(b). The ellipse 6 (cyan) corresponds to the peak indicated by the cyan marker.

a resonant scattering, the curve is naturally a Lorentzian and its width is a measure of how much "resonant" is the scattering. Therefore, the narrower is the peak, the more noticeable is the corresponding quasi-bound state. Thus, we can predict that $l = 0$ mode is characterized by more prominent trapping effects, compared to $l = -2$ mode.

In Fig. 3 we show the ξ coordinates of the first seven resonances and their associated polarization ellipses. The ellipse 6 (cyan curve) corresponds to the peak indicated by the cyan marker in Fig. 2(b).

Our main interest in this work is to correlate the scattering resonances with the generation of quasi-bound states. In this respect, we investigate in terms of density and current, all the illustrative regimes discussed above. The density function is defined as $\rho = \psi^\dagger \psi$ and, respectively, current as $\mathbf{j} = \psi^\dagger \boldsymbol{\sigma} \psi$. For the inside region of the QGD we substitute $\psi = \psi_i(r, \varphi)$ and, respectively, for the outside region $\psi = \psi_i(r, \varphi) + \psi_r(r, \varphi)$. First, we analyze the scattering regime indicated by marker 1 (black) in Fig. 2(b). According to the previous analysis, in terms of scattering efficiency, we do not expect to encounter here the generation of a quasi-bound state. Indeed, this prediction is confirmed by the density picture [Fig. 4(a)] which shows how the incident electronic wave diffracts on the GQD. In this way, the incident electron avoids the inner region of the dot and no quasi-bound state must be expected. The current [panel (b)] shows how the presence of the dot disrupts the propagation of the incident wave and also how the diffraction fringes are generated. The incident electron propagates eluding the dot and, even though a small amount of current may be observed inside, the current indicates that the electron only straightly passes the dot. Hence, there is not any quasi-bound state. The second investigation concerns the resonant excitation of $l = 0$ mode, see marker 2 (red) in Fig. 2(b). In this regime the electronic wave behaves fundamentally different. The density [Fig. 4(c)] shows a very interesting pattern. We can observe that the highest values are focused inside the dot and this indicates that the electron is in a quasi-bound state. We notice here a striking azimuthal asymmetry of the density. This counter-intuitive effect occurs due to the interference between the excited modes. In Supplementary information 2 [16] we present the density for each modes separately. We

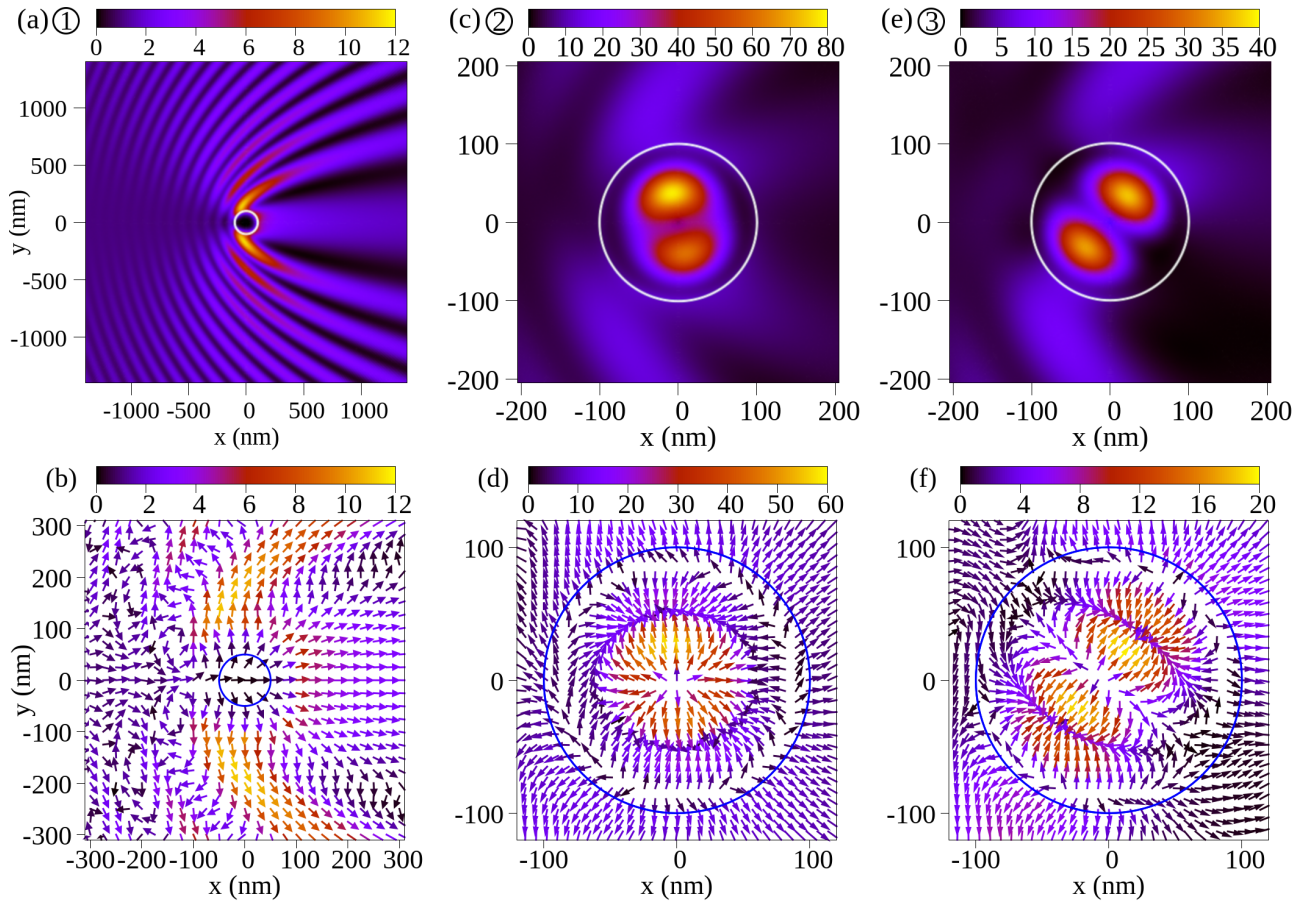


FIG. 4. Scattering analysis in terms of density and current. On each column, the upper panel shows the density, and respectively, the lower shows the current. The scattering regimes are those indicated by markers 1 (black), 2 (red) and 3 (blue) in Fig. 2(c). The spatial localization of the GQD is marked by white circle in the density plots and, respectively, blue circle in current plots.

can see in Fig. 2(b) that, besides $l = 0$, the $l = -2$ mode (blue curve) is resonantly excited, but with the peak slightly shifted. However, the tail of the $l = -2$ curve overlaps with the maximum of the $l = 0$ peak. Unlike the previous case, in the present regime [Fig. 4(d)] follows curved (vortex-like) trajectories and concentrates in those two zones where the density reaches the maximum values. This rotational flow of the current is responsible for the generation of the quasi-bound state. The last investigated case is assigned to the resonant excitation of $l = -2$ mode, see marker 3 (blue) in Fig. 2(b). First, we mention that the density values [Fig. 4(e)] are approximately twice as small as in the previous case and, as mentioned when discussed the scattering efficiency, this is related to the width of the resonance peak [compare blue curve with the red one in Fig. 2(b)]. On the other hand, also in this case, the interference of the excited modes translates in the azimuthal asymmetric density pattern. The current [Fig. 4(f)] behaves in the same fashion as in the previous studied case.

It is well known that the Brillouin zone of graphene con-

tains two nonequivalent Dirac K -points. However, since in our studied case the intervalley scattering is suppressed [27], it is enough to perform the study for only one valley. In Supplementary information 3 [16], we study the second valley case (K') and the conclusions are the same.

IV. CONCLUSIONS

In conclusion, we proved that by adjusting the polarization state and intensity of the applied light, we can control the excitation of quasi-bound states for certain well-defined scattering modes. The main findings were supported by correlating the abstract notion of scattering efficiency with density and current, which are the most illustrative tools used to describe the electron trapping process.

-
- [1] K. S. Novoselov, A. K. Geim, S. V. Morozov, D. Jiang, Y. Zhang, S. V. Dubonos, I. V. Grigorieva, and A. A. Firsov, *Science* **306**, 666 (2004).
- [2] M. I. Katsnelson, K. S. Novoselov, and A. K. Geim, *Nature Phys* **2**, 620–625 (2006).
- [3] N. Dombey, and A. Calogeracos, *Phys. Rep.* **315**, 41-58 (1999).
- [4] A. De Martino, L. Dell’Anna, and R. Egger, *Phys. Rev. Lett.* **98**, 066802 (2007).
- [5] P. Hewageegana, and V. Apalkov, *Phys. Rev. B* **77**, 245426 (2008).
- [6] J. Lee, D. Wong, J. Velasco Jr, J. F. Rodriguez-Nieva, S. Kahn, HZ. Tsai, T. Taniguchi, K. Watanabe, A. Zettl, F. Wang *et al.* *Nature Phys* **12**, 1032–1036 (2016).
- [7] C. Gutiérrez, L. Brown, CJ. Kim, J. Park, and A. N. Pasupathy, *Nature Phys* **12**, 1069–1075 (2016).
- [8] H. Yang, *Nature Phys* **12**, 994–995 (2016).
- [9] Y. Pan, H. Ji, XQ. Li, and H. Liu, *Sci Rep* **10**, 20426 (2020).
- [10] A. Pena, *Phys. Rev. B* **105**, 045405 (2022).
- [11] A. Pena, *Phys. Rev. B* **105**, 125408 (2022).
- [12] A. Pena, *Physica E Low Dimens. Syst. Nanostruct.* **141**, 115245 (2022).
- [13] M. El Azar, A. Bouhlal, and A. Jellal, <https://arxiv.org/abs/2301.11211>.
- [14] M. El Azar, A. Bouhlal, A. D. Alhaidari, and A. Jellal, <https://arxiv.org/abs/2308.12922>.
- [15] K. S. Novoselov, A. K. Geim, S. V. Morozov, D. Jiang, M. I. Katsnelson, I. V. Grigorieva, S. V. Dubonos, and A. A. Firsov, *Nature* **438**, 197–200 (2005).
- [16] Supplementary Material
- [17] A. H. Castro Neto, F. Guinea, N. M. R. Peres, K. S. Novoselov, and A. K. Geim, *Rev. Mod. Phys.* **81**, 109 (2009).
- [18] M. Loewe, F. Marquez and R. Zamora, *J. Phys. A: Math. Theor.* **45** 465303 (2012).
- [19] J. H. Shirley, *Phys. Rev. B* **138**, 979 (1965).
- [20] H. Li, B. Shapiro, and T. Kottos, *Phys. Rev. B* **98**, 121101(R) (2018).
- [21] C. Wurl, and H. Fehske, *Phys. Rev. A* **98**, 063812 (2018).
- [22] U. De Giovannini, and H. Hübener, *J. Phys. Mater.* **3** 012001 (2020).
- [23] V. Junk, P. Reck, C. Gorini, and K. Richter, *Phys. Rev. B* **101**, 134302 (2020).
- [24] J. Cserti, A. Pályi, and C. Péterfalvi, *Phys. Rev. Lett.* **99**, 246801 (2007).
- [25] R. L. Heinisch, F. X. Bronold, and H. Fehske, *Phys. Rev. B* **87**, 155409 (2013).
- [26] Schulz, C., Heinisch, R. L., and Fehske, H., *Quantum. Matter* **4**, 346–351 (2015).
- [27] S. V. Syzranov, M. V. Fistul, and K. B. Efetov, *Phys. Rev. B* **78**, 045407 (2008).

Supplementary material to the manuscript: Control of electron trapping effects in graphene quantum dots via light polarization state

SUPPLEMENTARY INFORMATION 1: DERIVATION OF DIRAC EQUATION SOLUTIONS

We study the model of a circular GQD of radius R exposed to an arbitrarily polarized light irradiation. We consider the GQD lying in the horizontal xy -plane, while the light beam is propagating on z -axis, at normal incidence on the dot. The system is schematically described in Fig. S1. The state of a light irradiated massless Dirac fermion is described by the 2D time-dependent

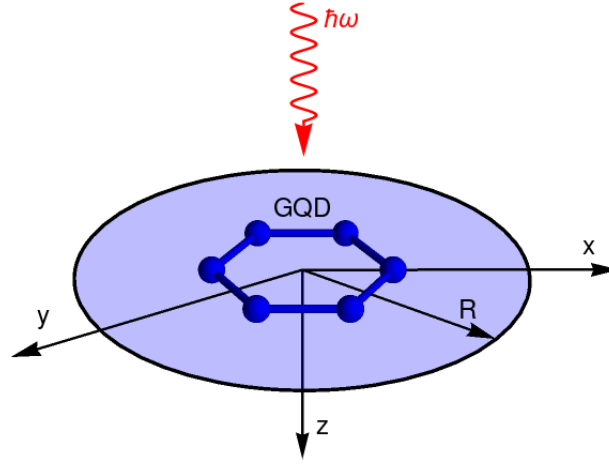


FIG. S1: Sketch of the studied system. The GQD of radius R is placed on the horizontal xy -plane, while the light beam ($\hbar\omega$) is propagating on z -axis, at normal incidence on the dot.

Dirac equation, which in polar coordinates reads (real spin degree of freedom neglected):

$$H(r, \varphi, t)\psi(r, \varphi, t) = i\hbar\partial_t\psi(r, \varphi, t); \quad (\text{S1})$$

$$H(r, \varphi, t) = H_0(r, \varphi) + H_{int}(t); \quad (\text{S2})$$

$$H_0(r, \varphi) = -iv_F\hbar\boldsymbol{\sigma} \cdot \nabla; \quad (\text{S3})$$

$$H_{int} = -ev_F\boldsymbol{\sigma} \cdot \mathbf{A}(t). \quad (\text{S4})$$

In equations above v_F is the Fermi velocity, \hbar the reduced Planck constant, $\nabla \equiv (\partial_r, \frac{1}{r}\partial_\varphi)$ the gradient operator, e the elementary charge constant and $\mathbf{A}(t)$ the vector potential of the light. $\boldsymbol{\sigma} = (\sigma_r, \sigma_\varphi)$ is the Pauli vector in polar coordinates, whose components read [1]:

$$\sigma_r = \begin{pmatrix} 0 & e^{-i\varphi} \\ e^{i\varphi} & 0 \end{pmatrix}; \quad \sigma_\varphi = \begin{pmatrix} 0 & -ie^{-i\varphi} \\ ie^{i\varphi} & 0 \end{pmatrix}. \quad (\text{S5})$$

Eq. (S3) represents the free Hamiltonian, while the interaction of the Dirac fermion with the applied light is expressed by the Hamiltonian term defined in Eq. (S4).

The state of an arbitrarily polarized plane wave may be expressed as a superposition of two circularly polarized plane waves with opposite helicities and complex amplitudes [2]:

$$\mathbf{A}(t) = [A_0e^{i\theta_A}(\hat{x} + i\hat{y}) + B_0e^{i\theta_B}(\hat{x} - i\hat{y})]e^{i\omega t}, \quad (\text{S6})$$

where $A_0(B_0)$ are real valued amplitudes and $e^{i\theta_A}(e^{i\theta_B})$ are arbitrarily chosen phase factors. For convenience we write

$$\mathbf{A}(t) = A_0e^{i\theta_A}[(\hat{x} + i\hat{y}) + \xi e^{i\theta}(\hat{x} - i\hat{y})]e^{i\omega t}; \quad \xi = \frac{B_0}{A_0}; \quad \theta = \theta_B - \theta_A. \quad (\text{S7})$$

Without losing generality we set $\theta_A = 0$. Generally speaking, Eq. (S7) represents an elliptical polarization state. The polarization ellipse is described as follows: ξ represents the ratio of the semi-major and, respectively, semi-minor axes by $|(1+r)(1-r)|$ and θ gives the ellipse orientation with respect to the reference frame.

From the physical point of view, of interest is only the real part of $\mathbf{A}(t)$, thus in what follows we make the substitution

$$\mathbf{A}(t) \rightarrow \text{Re}\{\mathbf{A}(t)\} = A_0[(\cos(\omega t) + \xi \cos(\omega t + \theta))\hat{\mathbf{x}} + (-\sin(\omega t) + \xi \sin(\omega t + \theta))\hat{\mathbf{y}}]. \quad (\text{S8})$$

Further, we exploit the time periodicity of the Hamiltonian $H(r, \varphi, t) = H(r, \varphi, t + T)$ with $T = 2\pi/\omega$ and employ the Floquet theorem [3–7] which ensures that the eigenvalue problem (S1) admits solutions of form

$$\psi(r, \varphi, t) = e^{-iWt/\hbar} \phi(r, \varphi, t). \quad (\text{S9})$$

Here, W is called *quasienergy* and is specified up to integer multiples of $\hbar\omega$ ($\tilde{W} = W + n\hbar\omega$; $n = -\infty, \dots, -1, 0, 1, \dots, \infty$) and $\phi(r, \varphi, t)$ is the *Floquet function*.

Introducing into the time-dependent Dirac equation (S1) the Floquet solution (S9), we are led to the following eigenvalue equation:

$$H_F(r, \varphi, t)\psi(r, \varphi, t) = W\psi(r, \varphi, t); \quad (\text{S10})$$

$$H_F(r, \varphi, t) = H(r, \varphi, t) - i\hbar\partial_t. \quad (\text{S11})$$

Here, $H_F(r, \varphi, t)$ is called *Floquet Hamiltonian*. Eq. (S10) is still time dependent. In what follows we present the derivation of an associated *stationary* problem in the approximation of an *effective Floquet Hamiltonian*.

We notice that the Floquet function is endowed with the same time periodicity as the Hamiltonian [$\phi(r, \varphi, t) = \phi(r, \varphi, t + T)$] and then we can eliminate the time dependence by making use of the Fourier series decomposition

$$H(r, \varphi, t) = \sum_{n=-\infty}^{\infty} H_n(r, \varphi); \quad (\text{S12})$$

$$\phi(r, \varphi, t) = \sum_{n=-\infty}^{\infty} \phi_n(r, \varphi). \quad (\text{S13})$$

The Fourier components read, respectively:

$$H_n(r, \varphi) = \frac{1}{T} \int_1^T e^{in\omega t} H(r, \varphi, t) dt; \quad (\text{S14})$$

$$\phi_n(r, \varphi, t) = \frac{1}{T} \int_1^T e^{in\omega t} \phi(r, \varphi, t) dt. \quad (\text{S15})$$

Manipulating Eqs. (S10)–(S15) we end with the following infinite system of coupled differential equations for the Fourier components $\phi_n(r, \varphi, t)$

$$\left(\sum_{m=-\infty}^{\infty} H_{m-n} + m\hbar\omega\delta_{mn} \right) \phi_m(r, \varphi, t) = W\phi_n(r, \varphi, t); \quad (\text{S16})$$

$$n = -\infty, \dots, 1, 0, 1, \dots, \infty,$$

called *Floquet system of equations*. For the case of a non-resonant interaction [8], characterized by a much higher energy of the light $\hbar\omega$ compared to the Dirac fermion energy scale, we can truncate the Floquet system and the problem reduces to the following eigenvalue equation [9, 10]:

$$(H_{eff} - W)\phi(r, \varphi) = 0; \quad (\text{S17})$$

$$H_F^{eff} = H_0 + \frac{1}{\hbar\omega}[H_{-1}, H_1]. \quad (\text{S18})$$

The commutator in Eq. (S18) expresses the virtual process of absorption/emission of one photon and, taking into consideration Eq. (S8), is readily derived as

$$[H_{-1}, H_1] = -(ev_F A_0)^2 (\xi^2 - 1) \sigma_z. \quad (\text{S19})$$

For simplicity we omitted the to specify the spatial dependence in Eqs. (S17)-(S19).

Taking into consideration Eqs. (S18) and (S19), Eq. (S17) translates as

$$\left[-i \left(\sigma_r \partial_r + \frac{1}{r} \sigma_\varphi \partial_\varphi \right) - \frac{1}{\lambda_{A_0}} (\xi^2 - 1) \sigma_z - \kappa \right] \phi(r, \varphi) = 0, \quad (\text{S20})$$

where we have introduced the notations

$$\lambda_{A_0} = \left(\frac{v_F e^2 A_0^2}{\hbar^2 \omega} \right)^{-1}; \quad \kappa = \frac{W}{v_F \hbar}. \quad (\text{S21})$$

Now our aim is to derive the expression for the unknown spinor $\phi(r, \varphi) = \left(\phi_A(r, \varphi), i\phi_B(r, \varphi) \right)^T$. In what follows we exploit the rotational symmetry of the Hamiltonian (S18), which guarantees the following commutation relation

$$[H_{eff}, J_z] = 0, \quad (\text{S22})$$

where $J_z = L_z + S_z$ is the total angular momentum operator with $L_z = -i\hbar\partial_\varphi$ the orbital angular momentum operator and, respectively, $S_z = (\hbar/2)\sigma_z$ the spin operator. Hence, we introduce the following ansatz:

$$\phi(r, \varphi) = \begin{pmatrix} \chi_A(r) e^{il\varphi} \\ i\chi_B(r) e^{i(l+1)\varphi} \end{pmatrix}, \quad (\text{S23})$$

which is a total angular momentum state, for the eigenvalue $(l + 1/2)\hbar$.

If we introduce Eq. (S23) into the homogeneous first order partial differential equation (S20), we obtain the following system of coupled first order differential equations for the unknown spinor components:

$$\partial_r \chi_A(r) - \frac{l}{r} \chi_A(r) - i \frac{\kappa \lambda_{A_0} - \xi^2 + 1}{\lambda_{A_0}} \chi_B(r) = 0; \quad (\text{S24a})$$

$$\partial_r \chi_B(r) + \frac{l+1}{r} \chi_B(r) + i \frac{\kappa \lambda_{A_0} + \xi^2 - 1}{\lambda_{A_0}} \chi_B(r) = 0. \quad (\text{S24b})$$

The system above may be decoupled, leading to the following second order homogeneous differential equation for $\chi_A(r)$:

$$\partial_r^2 \chi_A(r) + \frac{1}{r} \partial_r \chi_A(r) - \left(\frac{l^2}{r^2} + \frac{\kappa^2 \lambda_{A_0}^2 - (\xi^2 - 1)^2}{\lambda_{A_0}^2} \right) \chi_A(r) = 0. \quad (\text{S25})$$

The physical meaningful solutions of Eq. (S25) are the first kind Bessel functions of integer order l :

$$\chi_A(r) = J_l \left(-i \frac{r \sqrt{\lambda^2 k^2 - (\xi^2 - 1)^2}}{\lambda} \right). \quad (\text{S26})$$

The second component of $\phi(r, \varphi)$ is derived by introducing solution (S26) into Eq. (S24b):

$$\chi_B(r) = \frac{\lambda k + \xi^2 - 1}{\sqrt{\lambda^2 k^2 - (\xi^2 - 1)^2}} J_{l+1} \left(-i \frac{r \sqrt{\lambda^2 k^2 - (\xi^2 - 1)^2}}{\lambda} \right). \quad (\text{S27})$$

SUPPLEMENTARY INFORMATION 2: DENSITY AND CURRENT FOR EACH SCATTERING MODE

In Fig. S2 we present separately the density for each excited mode for the scattering regime indicated by marker 2 (red) in Fig. 2(b) in the manuscript (upper panel). Recall that the dominant mode $l = 0$ interferes with $l = -2$. See Fig. S2(a) and, respectively, Fig. S2(b) for their corresponding densities. Note that in the density plot we present only the inside region of the GQD, for a better visualization. Obviously, if we consider independently the excited modes, the azimuthal asymmetry discussed in the manuscript is absent.

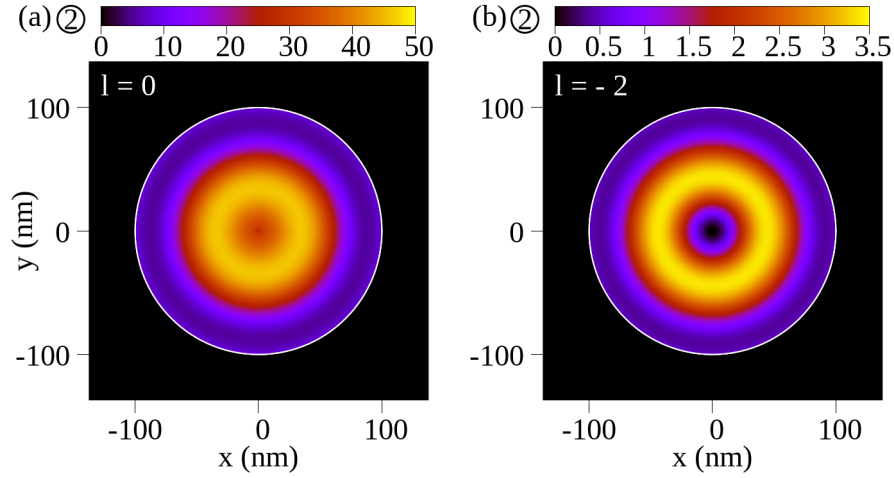


FIG. S2: Density plots shown separately for each excited mode corresponding to marker 2 (red) within Fig. 2(b) in the manuscript: (a) $l = 0$ and (b) $l = -2$. We consider only the inside region of the dot.

SUPPLEMENTARY INFORMATION 3: ANALYSIS FOR K' VALLEY

For the case of K' valley, we substitute into Dirac equation σ with σ^* , where "*" denotes the complex conjugate. The equation associated to the effective Floquet Hamiltonian becomes

$$\left[-i \left(\sigma_r \partial_r + \frac{1}{r} \sigma_\varphi \partial_\varphi \right) + \frac{1}{\lambda_{A_0}} (\xi^2 - 1) \sigma_z - \kappa \right] \phi(r, \varphi) = 0. \quad (\text{S28})$$

The sought spinor represents a state of well-defined total angular momentum for the eigenvalue $(l - 1/2)\hbar$:

$$\phi(r, \varphi) = \begin{pmatrix} \chi_A(r) e^{i(l-1)\varphi} \\ i\chi_B(r) e^{i\varphi} \end{pmatrix} \quad (\text{S29})$$

$$\chi_A(r) = J_{l-1} \left(-i \frac{r \sqrt{\lambda^2 k^2 - (\xi^2 - 1)^2}}{\lambda} \right); \quad (\text{S30})$$

$$\chi_B(r) = \frac{\lambda k + \xi^2 - 1}{\sqrt{\lambda^2 k^2 - (\xi^2 - 1)^2}} J_l \left(-i \frac{r \sqrt{\lambda^2 k^2 - (\xi^2 - 1)^2}}{\lambda} \right). \quad (\text{S31})$$

In Fig. S3 we present the scattering efficiency (Q) for the same parameters as for K -valley (in manuscript). The plots are identical for both valleys, with the difference that in the case of K' the excited modes are $-l$.

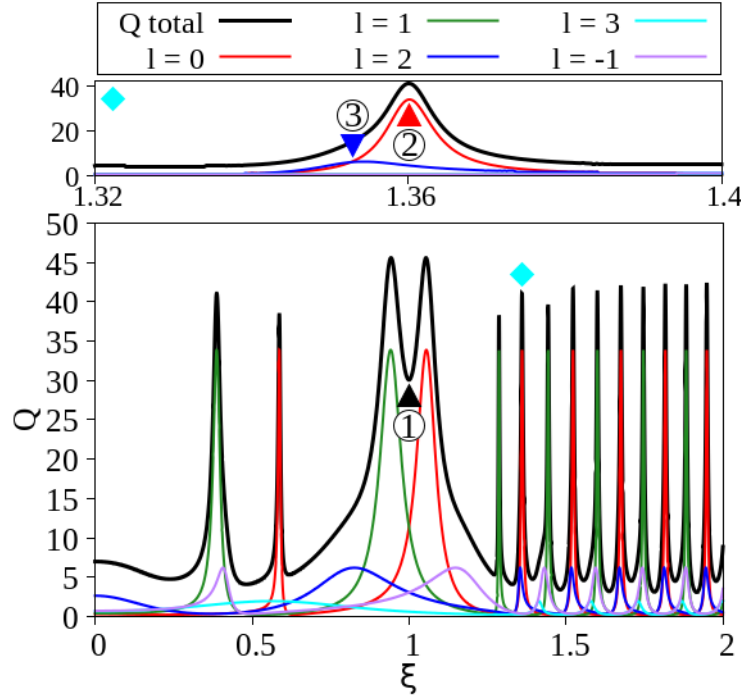


FIG. S3: Scattering efficiency (Q) as a function of ξ for the same parameters as for K' -valley.

In Fig. S4 we show the density and current for the scattering regimes indicated by markers 2 and 3 in Fig. S3 (the same as in the manuscript). Panels (a) and (c) presents the density and, respectively, (b) and (d) the current. In the K' -valley case the density and current patterns are reflected about x -axis. However, the effects of light irradiation are the same and the findings reveled in the manuscript are not affected by which valley we chose to study.

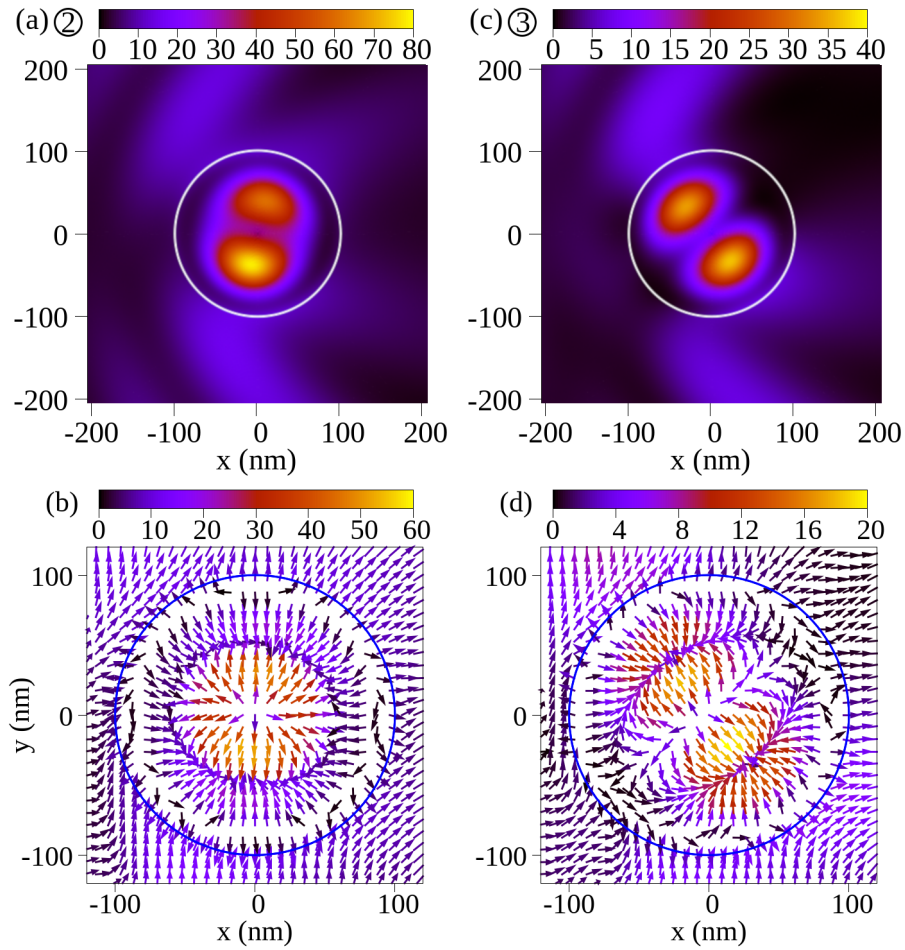


FIG. S4: Density and current for the scattering regimes indicated in Fig. S3: by marker 2, panels (a) and (b) and, respectively, by marker 3, panels (c) and (d).

-
- [1] M. Loewe, F. Marquez and R. Zamora, *J. Phys. A: Math. Theor.* **45** 465303 (2012).
[2] J. J. David, *Classical Electrodynamics* (New York :Wiley, 1999).
[3] J. H. Shirley, *Phys. Rev. B* **138**, 979 (1965).
[4] H. Li, B. Shapiro, and T. Kottos, *Phys. Rev. B* **98**, 121101(R) (2018).
[5] C. Wurl, and H. Fehske, *Phys. Rev. A* **98**, 063812 (2018).
[6] U. De Giovannini, and H. Hübener, *J. Phys. Mater.* **3** 012001 (2020).
[7] V. Junk, P. Reck, C. Gorini, and K. Richter, *Phys. Rev. B* **101**, 134302 (2020).
[8] K. Kristinsson, O. V. Kibis, S. Morina, and I. A. Shelykh, *Sci Rep* **6**, 20082 (2016).
[9] M.A. Sentef, M. Claassen, A.F. Kemper, B. Moritz, T. Oka, J.K. Freericks, and T.P. Devereaux, *Nat Commun* **6**, 7047 (2015).
[10] M. Vogl, M. Rodriguez-Vega, and G. A. Fiete, *Phys. Rev. B* **101**, 235411 (2020).